In Situ X-ray Microscopy Reveals Particle Dynamics in a NiCo Dry Methane Reforming Catalyst under Operating Conditions

Abbas Beheshti Askari, Mustafa al Samarai, Bruno Morana, Lukas Tillmann, Norbert Pfänder, Aleksandra Wandzilak, Benjamin Watts, Rachid Belkhou, Martin Muhler,* and Serena DeBeer*

Cite This: *ACS Catal.* 2020, 10, 6223−6230

Read Online

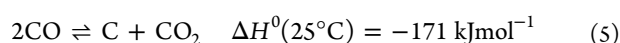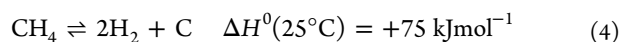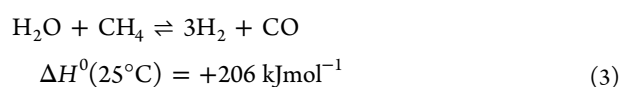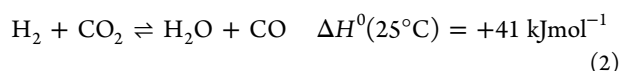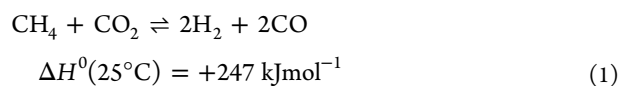ACCESS | Metrics & More | Article Recommendations | SI Supporting Information

ABSTRACT: Herein, we report the synthesis of a γ-Al_2O_3-supported NiCo catalyst for dry methane reforming (DMR) and study the catalyst using in situ scanning transmission X-ray microscopy (STXM) during the reduction (activation step) and under reaction conditions. During the reduction process, the NiCo alloy particles undergo elemental segregation with Co migrating toward the center of the catalyst particles and Ni migrating to the outer surfaces. Under DMR conditions, the segregated structure is maintained, thus hinting at the importance of this structure to optimal catalytic functions. Finally, the formation of Ni-rich branches on the surface of the particles is observed during DMR, suggesting that the loss of Ni from the outer shell may play a role in the reduced stability and hence catalyst deactivation. These findings provide insights into the morphological and electronic structural changes that occur in a NiCo-based catalyst during DMR. Further, this study emphasizes the need to study catalysts under operating conditions in order to elucidate material dynamics during the reaction.
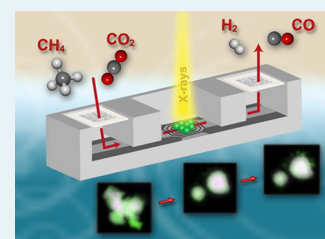
KEYWORDS: *in situ, heterogeneous catalysis, nanoreactor, methane reforming, X-ray spectroscopy, microscopy*

INTRODUCTION

The emission of greenhouse gases associated with the combustion of fossil fuels is believed to be the main cause of global warming.[1,2] Lowering the concentration of these gases is therefore a matter of utmost importance. An attractive approach would be the development of environmentally friendly processes capable of reusing these gases as feedstock for industrial processes. In this context, a reaction that has received much attention is dry methane reforming (DMR).[3−5] In this reaction, two major greenhouse gases, methane (CH_4) and carbon dioxide (CO_2), are converted into hydrogen (H_2) and carbon monoxide (CO), otherwise known as syngas. The DMR reaction (eq 1) together with the side reactions (eqs 2−5) proceeding under non-ideal conditions are reported below[6−8]

$$CH_4 + CO_2 \rightleftharpoons 2H_2 + 2CO$$
$$\Delta H^0(25°C) = +247 \text{ kJmol}^{-1} \quad (1)$$

$$H_2 + CO_2 \rightleftharpoons H_2O + CO \quad \Delta H^0(25°C) = +41 \text{ kJmol}^{-1} \quad (2)$$

$$H_2O + CH_4 \rightleftharpoons 3H_2 + CO$$
$$\Delta H^0(25°C) = +206 \text{ kJmol}^{-1} \quad (3)$$

$$CH_4 \rightleftharpoons 2H_2 + C \quad \Delta H^0(25°C) = +75 \text{ kJmol}^{-1} \quad (4)$$

$$2CO \rightleftharpoons C + CO_2 \quad \Delta H^0(25°C) = -171 \text{ kJmol}^{-1} \quad (5)$$

In the literature, various classes of materials, including noble metals, spinels, hydrotalcites, and supported base metals, have been reported as catalysts for the DMR process.[9−11] Among these catalysts, noble metals show the highest activity and stability toward this reaction but are economically not attractive.[12] In recent years, various studies focused on the development of late 3d transition metal-based systems as an alternative to costly noble metals for DMR catalysis.[9−11,13] Within this context, nickel (Ni)-based catalysts are promising candidates due to their relatively high activity and earth abundance. Nevertheless, the major drawback of monometallic Ni-based catalysts when compared to noble metal-based catalysts is their lower activity and higher susceptibility to deactivation due to coke formation via either methane cracking or the reverse Boudouard reaction.[14−19] In order to increase catalyst activity and stability, researchers have implemented various approaches including (i) depositing the catalytic active phase on different support materials,[20,21] (ii) reducing the catalyst, particle size,[22,23] (iii) developing bimetallic catalysts based on transition metals,[24−27] and (iv) transition metal-based core−shell nanoarchitectures.[28−30] It has been shown that core-shell systems have the ability to prevent metal sintering and decrease carbon formation, while the production
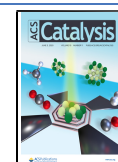
of bimetallic catalysts has been very successful in increasing the catalyst activity, stability, and selectivity. Among 3d transition metals, the addition of cobalt (Co) to Ni-based DMR catalysts results in the highest increase in activity. This has been ascribed to the optimal catalytic performance of the Ni/Co alloy.[31,32] Within this context, Zhang et al. investigated NiCo catalyst samples with various Ni and Co loadings and established that a lower Co concentration results in an increased catalytic activity and stability and prevents the coke formation side reaction to a large extent.[33] An operando X-ray absorption spectroscopy (XAS) study by Takanabe et al. revealed that Co increases the capacity of CO_2 adsorption, which eventually leads to carbon elimination from the catalyst surface.[34] Furthermore, in the same study, the presence of a homogeneous NiCo alloy was directly correlated to the DMR activity. This finding was supported by a combined in situ transmission electron microscopy (TEM) and X-ray photo-electron spectroscopy (XPS) study by Bonifacio and co-workers, which revealed that NiCo core—shell particles tend to form a homogeneous alloy at high temperatures (600 °C).[35] In addition, an ex situ TEM and in situ XPS study by Carenco et al. revealed that under reducing conditions and low temper-atures (270 °C) the morphology of NiCo particles changes into a structure consisting of NiCo alloy shell and a nickel-rich core.[36] From these studies and many others reported in the literature,[36–40] the formation of a NiCo alloy seems to play a crucial role in optimizing the DMR activity. However, none of these studies were performed at optimal operating temper-atures for DMR (>700 °C).[34] The differences between the particle morphology at low and high temperatures[35,36] suggest that it is necessary to follow the electronic structure and elemental distributions of Co and Ni during both the reductive activation step and under DMR conditions.

In general, the scarce information regarding the role of transition metals in methane reforming catalysis is mainly due to the lack of experimental techniques capable of simulta-neously probing the changes in the electronic structure and visualizing the morphology of the active phase under operating conditions. Within this context, scanning transmission X-ray microscopy (STXM) is a promising technique whereby soft X-ray spectroscopy is combined with 2D microscopy. Recently, it has been reported that by employing microfabricated monolithic nanoreactors,[41] together with a specifically designed in situ gas-phase setup, the changes in the particle morphology and electronic structure of the catalytic active phase can be imaged and probed under operating con-ditions.[42–44] The specific combination of nanoreactors and an in situ gas-phase setup developed for this study allowed simultaneously operating at temperatures (750 °C) and pressures (3.0 bar) that are higher than those until now reported for in situ STXM studies.[44,45] This advancement is key for studying catalysts under industrially relevant con-ditions. Herein, we first present a synthetic method for a bimetallic alumina-supported NiCo DMR catalyst followed by in situ STXM characterization of the catalyst performed during the reductive activation step and under DMR operating conditions. To the best of our knowledge, this is the first in situ STXM study of a bimetallic DMR catalyst. These data are crucial for the understanding of the catalytic dynamics involved in the reforming of methane and thus are fundamental to the development of catalysts with superior properties.

■ EXPERIMENTAL SECTION

Catalyst Synthesis. For the synthesis, cobalt(II) acetate tetrahydrate (>98%, Sigma Aldrich), nickel(II) acetate tetrahydrate (99.998%, Sigma Aldrich), ammonium oxalate monohydrate (98%, Alfa Aesar), methanol (99%, Alfa Aesar), 1-hexanol (99%, Alfa Aesar), and *n*-hexane 99% gamma alumina catalyst support (surface area of 200 m^2/g, Alfa Aesar) were employed.

The $NiCoO_x/\gamma Al_2O_3$ catalyst was synthesized according to the modified reverse micellar method.[46,47] The advantage of this synthesis method is that it enables the production of a bimetallic catalyst with controlled size and elemental ratios incorporating late transition metals. Other methods are mainly focused on the synthesize of small particles with the aim of increasing the activity[22,23,48] and limiting coke formation.[49,50] In contrast, for STXM characterizations, where the spatial resolution is limited, larger particles are desired. By using the modified micellar method, we successfully produced highly active and stable particles, which have the ideal size for STXM characterizations. The first step in the production of the bimetallic catalyst involved preparing four different mixtures. Herein, 2.3 g of ammonium oxalate monohydrate, 2.0 g of nickel acetate tetrahydrate, and 0.71 g of cobalt acetate tetrahydrate were separately dissolved in 15 mL of water and stirred for 15 min to obtain three different solutions. The fourth mixture was prepared by mixing and stirring 0.9 g of cetyltrimethylammonium bromide, 9 mL of hexanol, and 12.6 mL of hexane for 20 min. This mixture was divided into three equal parts, and each of these was then added to the first three mixtures and stirred for another 20 min. In the last stage, all solutions were added together and stirred for 48 h to obtain the bimetallic catalyst. The produced catalyst was purified by centrifuging at 5500 rpm for 5 min and washed with a mixture of 30 mL of methanol and 30 mL of chloroform. This procedure was followed by centrifugation at 5500 rpm for 10 min and drying at 50 °C for 12 h. To deposit the bimetallic catalyst on a support, 2.5 mL of water was added to the prepared catalyst and 0.8 g of γ-Al$_2$O$_3$ was added to the solution. This was then stirred for 20 min and dried at 90 °C for 12 h. The final phase of this process included calcining the supported catalyst at 400 °C for 10 h in an argon atmosphere. In the study by Fakeeha and Al-Fatesh, it was shown that a low calcination temperature results in a large surface area of Ni-based DMR catalysts.[51] This simple method allows the production of a wide variety of catalysts by selecting the desired metal acetates. In addition, the size of the active phase can be tuned by varying the amount of water and metal acetates used in this process. Figure S1 shows the complete synthesis route used in this study to produce the $NiCoO/\gamma$-Al$_2$O$_3$ catalyst.

Scanning Transmission Electron Microscopy (STEM) Experiments. For the STEM measurements, a polymer-coated Cu TEM grid was immersed in the dry catalyst powder. The morphology and elemental distribution of the catalyst were imaged by using the Hitachi HD-2700 spherical aberration-corrected STEM. Images were acquired with an acceleration voltage of 200 kV. In addition, energy-dispersive X-ray (EDX) spectra were recorded with an EDAX Octane T Ultra W 200 mm^2 SDD attached to the STEM microscope.

Activity Measurements. For the activity measurements, the setup described in the work of Muhler et al. was employed.[52] The effluent gas was analyzed using an Agilent
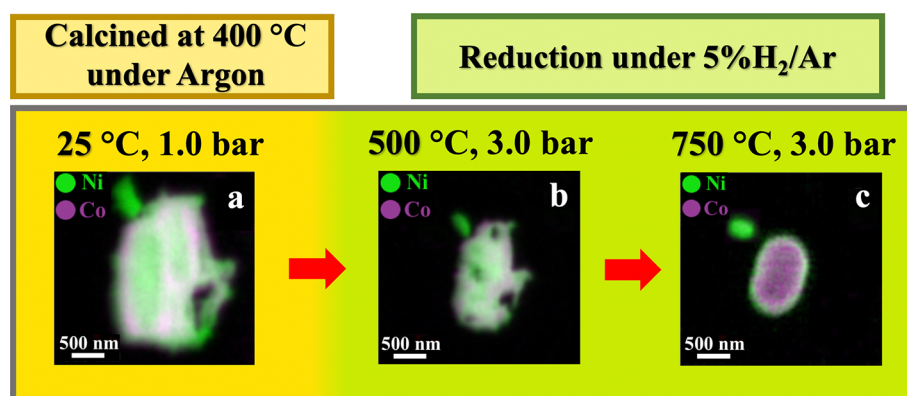
Figure 1. Elemental composition maps showing the distribution of Ni (in green) and Co (in violet) for (a) freshly calcined particles, (b) following the reduction step at 500 °C under 5% H_2 in Ar, where the Ni and Co oxides are reduced, and (c) at 750 °C and under 5% H_2 in Ar flow where the Ni and Co Al_2O_4 are fully reduced. This last image confirms the elemental segregation within the large agglomerates upon full reduction.
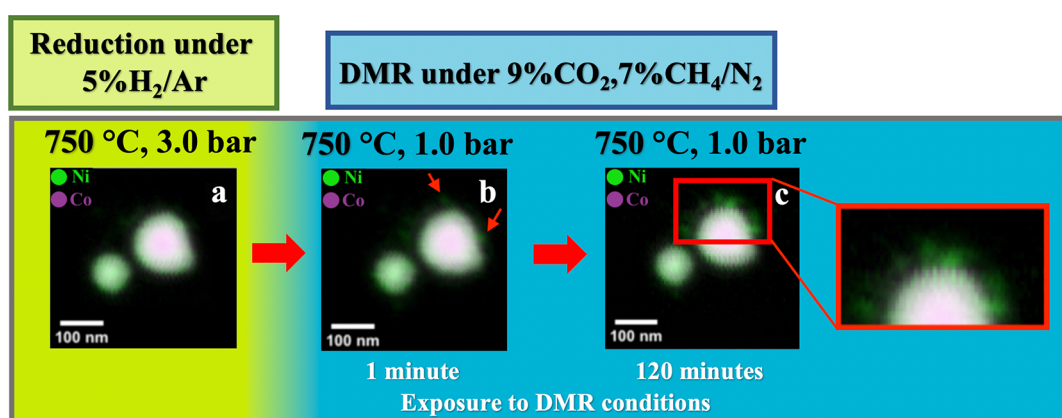

Figure 2. Elemental composition maps of the nanoparticle under study. (a) Acquired after reduction and confirming the elemental segregation within the large agglomerates. (b) Acquired after exposure to DMR conditions for 1 minute and (c) 120 minutes. In (b) the increase of the Ni concentration in certain locations of the surface is visible and indicated with red arrows. In (c) the formation of Ni branches starting form the surface of the nanoparticle is visible and emphasized in the close up.

3000 Micro-GC equipped with PLOT-Q and Molsieve 5A PLOT columns and a TCD for quantification. The gases employed for the activity measurements were 10% H_2 diluted in N_2 (purity, 99.999%), CH_4 (purity, 99.995%), CO_2 (purity, 99.995%), and N_2 (purity, 99.999%).

The first step of the activity experiments involved sieving 50 mg of the supported NiCo catalyst to obtain nanoparticles smaller than 200 μm. Subsequently, these were loaded in the fixed-bed reactor and activated by flowing 10% H_2 in N_2 (flow rate of 100 mL min^{-1}), for a time of 20 min and with a set temperature of 850 °C. Finally, the activity was measured for 15 h under DMR conditions, that is, by flowing a gas mixture of 7% CH_4 and 9.5% CO_2 in N_2 (flow rate of 490 mL min^{-1}). We note that due to the configuration of the employed setup and more interestingly to the endothermicity of the DMR reaction, causing by itself a cold spot in the center of the fixed-bed reactor, the temperature in the center of the bed deviates from the set temperature.[52] Therefore, during our activity measurements, a temperature of 800 °C was set to obtain an approximate temperature of 750 °C at the catalyst.

Temperature-Programmed Reduction (TPR) Measurements. The TPR profile was recorded in a quartz cell filled with 81.9 mg of the calcined catalysts. The sample was heated up to 850 °C with a rate of 6 °C/min in a continuous flow of 4.6% H_2 in Ar (purity, 99.99), adding up to a total

volume of 84.1 mL min^{-1}. The H_2 consumption was determined by using a thermal conductivity analyzer (Hydros 100, Rosemount).

STXM. The STXM measurements for the particle shown in Figure 1 were performed at the PolLux beamline of the Paul Scherrer Institute,[53,54] while the particle shown in Figure 2 was measured at the Hermes beamline at SOLEIL synchrotron radiation facility. The spatial resolution of the zone plates was 35 nm for both beamlines. The first stage of the STXM experiment involved measuring the calcined sample. Next, the sample was exposed to reducing conditions (5% H_2 in Ar) while gradually increasing the temperature from 25 to 750 °C. During the activation process, the pressure was increased up to 3.0 bar with the aim of accelerating the reduction. Additional measurements performed at 1.5 bar and 500 °C/750 °C showed only minor changes in the particle size and no detectable variations in its morphology (see the Supporting Information Figure S2). Finally, the sample was investigated under DMR conditions, that is, by flowing a gas mixture of 7% CH_4 and 5% CO_2 diluted in N_2, at a pressure of 1.0 bar, and at temperature of 750 °C.

■ RESULTS

STEM. STEM images of the calcined sample displayed the formation of large agglomerates consisting of coalesced
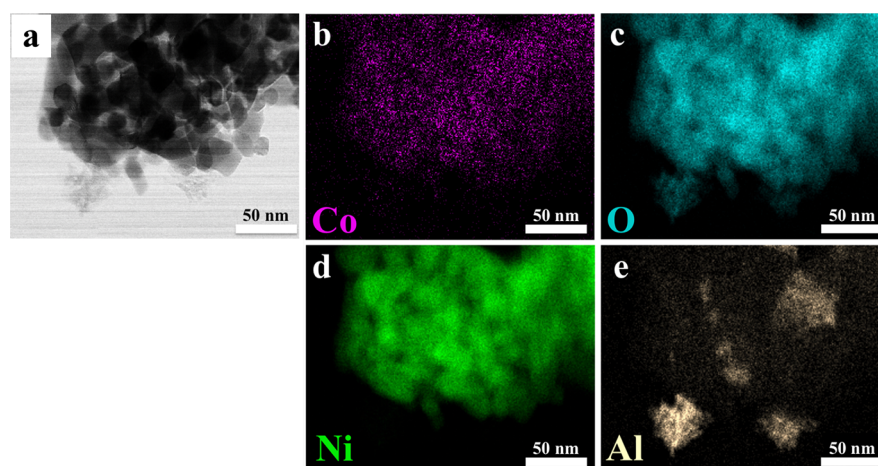
Figure 3. (a) Bright-field STEM image of the catalyst calcinated at 400 °C. (b−e) STEM-EDX elemental mapping images of Co, O, Ni, and Al shown in violet, blue, green, and yellow, respectively. (c) Measured oxygen signal originating from the metal oxides and the alumina.

nanoparticles in the range of 5−20 nm (Figure 3a and Figure S3). In addition, energy-dispersive X-ray spectroscopy (EDX) data showed the distribution of Co (violet) and Ni (green) oxides (Figure 3b−d) on the alumina support (yellow). Moreover, it is shown that both Ni and Co are not homogeneously distributed throughout the large agglomerates, and specific domains with mainly a NiO character are also encountered as determined from X-ray diffraction (XRD) (Figure S4). Furthermore, the metal loadings in atomic % for the $NiCoO_x/\gamma-Al_2O_3$ catalyst were predetermined from the bulk EDX analysis and corresponded to 56.4% (oxygen), 1.1% (cobalt), 9.2% (nickel), and 33.3% (aluminum). In addition, the Ni/Co ratio in this sample was close to 9:1 (Figure S5).

TPR and Catalytic Activity Tests. Prior to the in situ STXM experiment, the TPR profile and the catalytic activity for the $NiCoO/\gamma-Al_2O_3$ DMR catalyst were measured (Figure S6). The TPR profile shows the presence of two clear reduction peaks and suggests the reduction of metal oxides in the temperature range of 250−500 °C. The first peak at 265 °C is assigned to the reduction of Co^{3+} species to Co^{2+}, whereas the main peak at 325 °C is assigned to the reduction of Ni^{2+} and Co^{2+} to their metallic states.[55−58] Furthermore, these data indicate that full reduction of the metal oxides into the metallic state already occurs at temperatures lower than 500 °C. Next, the DMR activity of the $NiCoO/\gamma-Al_2O_3$ catalyst was investigated at a lab scale via a fixed-bed reactor by loading 50 mg of the catalyst particles that were sieved down to <200 μm. In the first stage of the experiment, the catalyst was activated by performing a reduction treatment under 10% H_2 in N_2 by setting the temperature to 850 °C. The catalyst was then cooled down by setting the temperature to 800 °C, and after switching to the DMR gas mixture (7% CH_4 & 9.5% CO_2 in N_2), the DMR activity was measured on stream for 15 h. The degree of CH_4 and CO_2 conversion after 2 h stabilized at 86 and 77%, respectively (Figure 4). In addition, the yields for H_2 and CO were calculated using eq S1 and corresponded to ~78 and ~80%, respectively. The activity of the $NiCoO/\gamma-Al_2O_3$ DMR catalyst in terms of CH_4 conversion is of the same order of magnitude as that exhibited by bimetallic NiCo catalysts in the literature (75−90%), which was found to exceed that of monometallic Ni or Co DRM catalysts (<70%).[21,35,36] These findings hint to the synergistic effect between Ni and Co in the bimetallic NiCo DMR
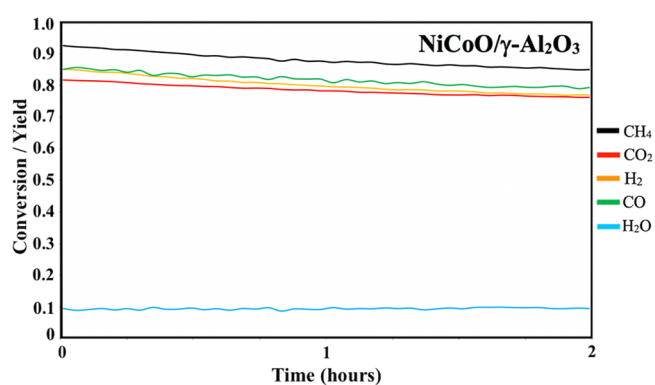

Figure 4. Activity measurements for the $NiCoO/\gamma-Al_2O_3$ DMR catalyst (conversion/yield fractions during the DMR experiment under 7% CH_4 and 9.5% CO_2 in N_2 and a flow rate of 490 mL min^{-1}). Due to the configuration of the setup and the endothermicity of the DMR reaction, the oven temperature was set to 800 °C to achieve a temperature of ~750 °C at the center of the bed. Prior to the DMR activity measurements, the catalyst was treated for 30 min under 10% H_2 in N_2 with a flow rate of 100 mL min^{-1}.

catalyst. Furthermore, Figure S7 and Table S1 show, respectively, the activity measurement results and corresponding conversion/yield values, after exposing the catalyst to DMR conditions for 15 h.

STXM. For the STXM measurements, the X-ray transmission signal of a selected particle was acquired at both Ni (in green) and Co (in violet) L-edges for (I) the freshly calcined sample, (II) during reduction with 5% H_2 in Ar, and (III) through the DMR process under 7% CH_4 and 9.5% CO_2 in N_2. Figure S8 illustrates that multiple particles were investigated to confirm the reproducibility of the in situ STXM results. The average lateral dimensions and thicknesses of the selected calcined catalyst particles were in the order of 0.4−1.2 μm and 0.2−0.3 μm, respectively. Each of the spectral elemental images were obtained by subtracting the pre-edge spectral elemental map from that obtained at the L_3-edge maximum. The elemental composition maps presented in Figure 1a−c are collected from an identical spot. Furthermore, the corresponding Co and Ni L_3-edge XAS spectra are shown in Figure 5. For the sake of comparison, L_3-edge XAS spectra of the metallic Ni and Co oxides are also included in Figure 5.
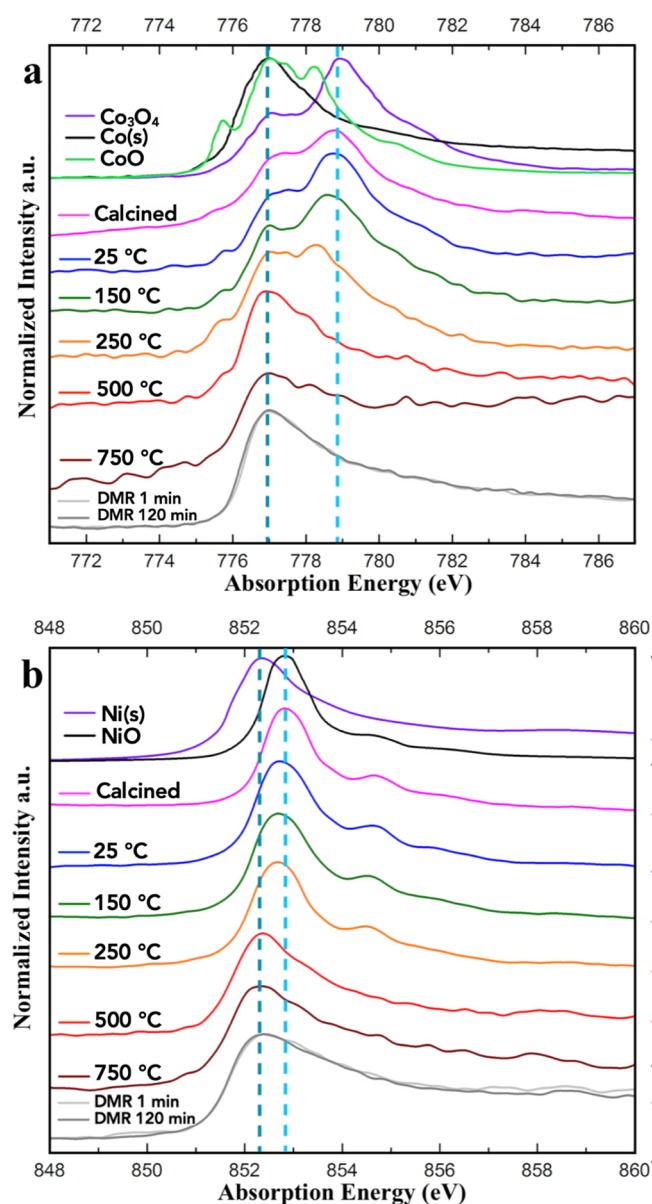
Figure 5. (a) Co L$_3$-edge spectrum of the NiCoO/γ-Al$_2$O$_3$ sample collected under operating conditions. The L$_3$-edge of the calcined catalyst has the same shape and energy position when compared to Co$_3$O$_4$. Under reducing conditions at 500 °C, the Co$_3$O$_4$-like compound is converted into metallic Co. (b) Collection of Ni L$_3$-edge spectra of the fresh catalyst having the same shape and energy position if compared to NiO. Under DMR conditions, both the Ni and Co stay reduced.

In general, the elemental composition maps for the freshly calcined sample (Figure 1a) show a rather inhomogeneous distribution of Ni and Co on the γ-Al$_2$O$_3$ support. This observation is further supported by the individual elemental composition maps of Co and Ni acquired for the same calcined particle (Figure S9). There are, however, some Ni-rich regions in the calcined catalyst, consistent with the corresponding STEM-EDX data (Figure 3). Based on a comparison with reference spectra, the formation of Co$_3$O$_4$ (2xCo^{3+} O$_h$ and 1xCo^{2+} T$_d$) and NiO (Ni^{2+} O$_h$) species, as a result of the calcination process, is confirmed as reported in other studies.[24,59]

Next, the catalyst was activated by increasing the temperature stepwise from 25 °C to 750 °C under a continuous 5% H$_2$ in Ar flow. In order to accelerate the reduction process, the pressure was set to 3.0 bar. The corresponding Co and Ni L$_3$-edges are shown in Figure 5 and Figures S10 and S11. At the initiation of the reduction step, the pressure was increased to 3.0 bar to accelerate the reduction process. At 250 °C, the Ni L$_3$-edge remains essentially unaffected, indicating that Ni^{2+} is still present. However, the Co L$_3$-edge has changed quite significantly both in the multiplet structure and in the average energy. The observed changes are consistent with the reduction of the Co^{3+} O$_h$ sites to most probably octahedrally coordinated Co^{2+} oxide. These results are in agreement with the TPR data (Figure S6) and with literature studies, where the partial reduction of Co$_3$O$_4$ was found to occur at a relatively lower temperature compared with the Ni site.[60,61] The most prominent changes in the L-edge spectra are observed at 500 °C. At this temperature, the shift in both Co and Ni L$_3$-edges together with the resulting spectral shape indicates the full reduction of the metal oxides to their metallic state. This result is again consistent with the measured TPR profiles (see Figure S6). Furthermore, Figure 1b shows that at 500 °C, the morphology and elemental distribution of the NiCo particle are altered. The formation of voids within the particle can be seen, which may be a result of restructuring upon loss of oxygen from the lattice under reducing conditions.[62,63] Figure S2 reveals that increasing the reduction pressure to 3.0 bar at 500 °C results in a minor decrease in the particle size.

In the second phase of the reduction process, performed at 750 °C, both the Co and Ni L$_3$-edges remain unchanged relative to the data acquired at 500 °C (Figure 5), thus supporting the full conversion of the metal oxides at 500 °C into their metallic species. However, the elemental composition maps shown in Figure 1c display a rather dramatic change in the elemental distribution of the active phase with Co migrating inward and a Ni-rich shell forming on the surface of the large agglomerate. The elemental composition maps shown in Figure 1 and Figure S12 show that in this step, the formed structure consists of two parts: (I) the surface, made of only Ni, and (II) the core, consisting of both Co and Ni. This demonstrates the increase in surface mobility of Ni and Co at high temperature and under 5%H$_2$ in Ar flow. Figure S2 shows that increasing the pressure from 1.5 to 3.0 bar only slightly influences the particle morphology, with this becoming slightly more spherical. While previous studies have suggested that alloy formation between Ni and Co is key to optimizing the DMR activity and stability,[29,37,64,65] for the system under study, we show that elemental segregation to form a Ni-rich surface is involved in the activation of the catalyst. We note that previous in situ XPS studies by Wu et al.[37] of a related NiCo catalyst, obtained by the wet impregnation method, indicated that Co migrates inward during the reduction of NiCo. Further they showed that upon the completion of reduction, the surface of the nanoparticle is a 50:50 mixture of Co and Ni.[37] However, due to the intrinsic differences between our catalyst and that studied by Wu, such comparisons must be made with caution. Regardless, these results highlight the power of spectromicroscopy for identifying morphological, structural and element distribution changes in nanoparticles during operating conditions.

Finally, under DMR reaction conditions, we focused on another NiCo particle with much smaller dimensions in order to precisely follow the changes in morphology and in the

elemental distribution. Herein, elemental composition maps and L_3-edge XAS spectra were obtained during the DMR reaction at 750 °C under 7% CH_4 and 9.5% CO_2 in N_2 at (I) 1 minute and (II) 120 min exposure time. The data collected after 1 min exposure to the DMR conditions clearly indicate that the segregated structure is preserved (Figure 2b) and that both Ni and Co remain fully reduced based on the L_3-edge spectra (Figure 5). Furthermore, Figure 2a,b reveals that changing the pressure from 3.0 to 1.0 bar does not influence the particle morphology and size. However, a closer inspection of Figure 2b reveals that in for the large NiCo particle, the Ni concentration has increased in certain locations on the surface, as indicated with red arrows. After 120 min under DMR conditions, the Ni and Co are still reduced, as seen from the L-edges but the formation of Ni-rich branches at the surface of the particle is observed (Figure 2c). This unexpected event may be associated with the growth of filamentous carbon on the surface of the catalytically active sites.[66,67] This result is consistent with that of Takanabe et al. where it was demonstrated that carbonaceous species are removed at a slower rate on pure Ni surfaces, which ultimately leads to deactivation due to carbon deposition.[34]

CONCLUSIONS

In summary, we have successfully developed a modified route for the controlled synthesis of a NiCo catalyst with high activity and stability toward the DMR reaction. Importantly, the synthesis procedure produced large particles, which are amenable to studies by STXM. In situ STXM measurements show that while in the calcined form, the particles exhibit an inhomogeneous distribution of Ni and Co, and during the reductive activation step at 750 °C (5% H_2/Ar), a clear elemental segregation is observed; with Co migrating toward the center of the agglomerated nanoparticles and Ni forming a shell on the outer surface of the particle. The segregated structure is preserved during DMR, suggesting that Ni is the primary active site, while the more readily oxidized Co may serve as an electron donor to Ni during catalysis. The dynamics of morphology and elemental distribution of the nanoparticle highlights a mechanism by which the synergistic interaction between the metals is optimized to maximize catalytic activity and minimize coking.[68]

This study highlights the ability of in situ STXM to monitor the evolution of particle morphology, elemental distribution, and electronic structure under operating conditions. In this respect, the employed in situ setup represents a major technological advancement, as it enables the types of industrially relevant processes that can be studied with STXM to be greatly expanded. As such, we are convinced that this method development, by providing a means to evaluate catalytic mechanisms and deactivation processes, will enable important advances in the understanding of heterogeneous catalytic processes in general. We thus believe that in the future, in situ STXM will provide important contributions toward knowledge-based catalytic design.

ASSOCIATED CONTENT

Ⓢ Supporting Information

The Supporting Information is available free of charge at https://pubs.acs.org/doi/10.1021/acscatal.9b05517.

Additional data obtained from STEM, XRD, TPR, activity tests, and STXM elemental composition maps (PDF)

AUTHOR INFORMATION

Corresponding Authors

Martin Muhler − *Max Planck Institute for Chemical Energy Conversion, Mülheim an der Ruhr D-45470, Germany; Laboratory of Industrial Chemistry, Ruhr-University Bochum, Bochum D-44801, Germany;* ⓞ orcid.org/0000-0001-5343-6922; Email: muhler@techem.rub.de

Serena DeBeer − *Max Planck Institute for Chemical Energy Conversion, Mülheim an der Ruhr D-45470, Germany;* ⓞ orcid.org/0000-0002-5196-3400; Email: serena.debeer@cec.mpg.de

Authors

Abbas Beheshti Askari − *Max Planck Institute for Chemical Energy Conversion, Mülheim an der Ruhr D-45470, Germany*

Mustafa al Samarai − *Max Planck Institute for Chemical Energy Conversion, Mülheim an der Ruhr D-45470, Germany*

Bruno Morana − *NanoInsight, 2628 CT Delft, The Netherlands*

Lukas Tillmann − *Laboratory of Industrial Chemistry, Ruhr-University Bochum, Bochum D-44801, Germany*

Norbert Pfänder − *Max Planck Institute for Chemical Energy Conversion, Mülheim an der Ruhr D-45470, Germany*

Aleksandra Wandzilak − *Max Planck Institute for Chemical Energy Conversion, Mülheim an der Ruhr D-45470, Germany*

Benjamin Watts − *Paul Scherrer Institute, Villigen 5232, Switzerland*

Rachid Belkhou − *Synchrotron SOLEIL, Gif-sur-Yvette Cedex F-91192, France*

Complete contact information is available at:
https://pubs.acs.org/10.1021/acscatal.9b05517

Notes

The authors declare no competing financial interest.

REFERENCES

(1) Barelli, L.; Ottaviano, A. Solid Oxide Fuel Cell Technology Coupled With Methane Dry Reforming: A Viable Option For High Efficiency Plant With Reduced CO_2 Emissions. *Energy* **2014**, *71*, 118−129.

(2) Dufour, J.; Serrano, D. P.; Galvez, J. L.; Moreno, J. L.; García, C. Life Cycle Assessment Of Processes For Hydrogen Production. Environmental Feasibility And Reduction Of Greenhouse Gases Emissions. *Int. J. Hydrogen Energy* **2009**, *34*, 1370−1376.

(3) Das, S.; Shah, M.; Gupta, R. K.; Bordoloi, A. Enhanced Dry Methane Reforming Over Ru Decorated Mesoporous Silica And Its Kinetic Study. *J. CO2 Util.* **2019**, *29*, 240−253.

(4) Świrk, K.; Gálvez, M. E.; Motak, M.; Grzybek, T.; Rønning, M.; Da Costa, P. Syngas Production From Dry Methane Reforming Over

Yttrium-Promoted Nickel-KIT-6 Catalysts. *Int. J. Hydrogen Energy* **2019**, *44*, 274−286.

(5) Li, X.; Li, D.; Tian, H.; Zeng, L.; Zhao, Z.-J.; Gong, J. Dry Reforming Of Methane Over Ni/La$_2$O$_3$ Nanorod Catalysts With Stabilized Ni Nanoparticles. *Appl. Catal., B* **2017**, *202*, 683−694.

(6) Lavoie, J. M. Review On Dry Reforming Of Methane, A Potentially More Environmentally-Friendly Approach To The Increasing Natural Gas Exploitation. *Front. Chem.* **2014**, *2*, 81.

(7) Wang, Y.; Yao, L.; Wang, S.; Mao, D.; Hu, C. Low-Temperature Catalytic CO$_2$ Dry Reforming Of Methane On Ni-Based Catalysts: A Review. *Fuel Process. Technol.* **2018**, *169*, 199−206.

(8) Serrano-Lotina, A.; Rodríguez, L.; Muñoz, G.; Daza, L. Biogas Reforming On La-Promoted NiMgAL Catalysts Derived From Hydrotalcite-Like Precursors. *J. Power Sources* **2011**, *196*, 4404−4410.

(9) Muraza, O.; Galadima, A. A Review On Coke Management During Dry Reforming Of Methane. *Int. J. Energy Res.* **2015**, *39*, 1196−1216.

(10) Usman, M.; Wan Daud, W. M. A.; Abbas, H. F. Dry Reforming Of Methane: Influence Of Process Parameters—A Review. *Renewable Sustainable Energy Rev.* **2015**, *45*, 710−744.

(11) Dębek, R.; Zubek, K.; Motak, M.; Da Costa, P.; Grzybek, T. Effect Of Nickel Incorporation Into Hydrotalcite-Based Catalyst Systems For Dry Reforming Of Methane. *Res. Chem. Intermed.* **2015**, *41*, 9485−9495.

(12) Pakhare, D.; Spivey, J. A Review Of Dry (CO$_2$) Reforming Of Methane Over Noble Metal Catalysts. *Chem. Soc. Rev.* **2014**, *43*, 7813−7837.

(13) Medeiros, R. L. B. A.; Macedo, H. P.; Melo, V. R. M.; Oliveira, Â. A. S.; Barros, J. M. F.; Melo, M. A. F.; Melo, D. M. A. Ni Supported On Fe-Doped MgAl$_2$O$_4$ For Dry Reforming Of Methane: Use Of Factorial Design To Optimize H$_2$ Yield. *Int. J. Hydrogen Energy* **2016**, *41*, 14047−14057.

(14) Margossian, T.; Larmier, K.; Kim, S. M.; Krumeich, F.; Fedorov, A.; Chen, P.; Müller, C. R.; Copéret, C. Molecularly Tailored Nickel Precursor And Support Yield A Stable Methane Dry Reforming Catalyst With Superior Metal Utilization. *J. Am. Chem. Soc.* **2017**, *139*, 6919−6927.

(15) Baudouin, D.; Rodemerck, U.; Krumeich, F.; de Mallmann, A.; Szeto, K. C.; Ménard, H.; Veyre, L.; Candy, J.-P.; Webb, P. B.; Thieuleux, C.; Copéret, C. Particle Size Effect In The Low Temperature Reforming Of Methane By Carbon Dioxide On Silica-Supported Ni Nanoparticles. *J. Catal.* **2013**, *297*, 27−34.

(16) Carenco, S. Describing Inorganic Nanoparticles In The Context Of Surface Reactivity And Catalysis. *Chem. Commun.* **2018**, *54*, 6719−6727.

(17) Gonzalez-delaCruz, V. M.; Pereñiguez, R.; Ternero, F.; Holgado, J. P.; Caballero, A. In Situ XAS Study Of Synergic Effects On Ni−Co/ZrO$_2$ Methane Reforming Catalysts. *J. Phys. Chem. C* **2012**, *116*, 2919−2926.

(18) San-José-Alonso, D.; Juan-Juan, J.; Illán-Gómez, M. J.; Román-Martínez, M. C. Ni, Co And Bimetallic Ni−Co Catalysts For The Dry Reforming Of Methane. *Appl. Catal., A* **2009**, *371*, 54−59.

(19) Wang, H.; Blaylock, D. W.; Dam, A. H.; Liland, S. E.; Rout, K. R.; Zhu, Y.-A.; Green, W. H.; Holmen, A.; Chen, D. Steam Methane Reforming On A Ni-Based Bimetallic Catalyst: Density Functional Theory And Experimental Studies Of The Catalytic Consequence Of Surface Alloying Of Ni With Ag. *Catal. Sci. Technol.* **2017**, *7*, 1713−1725.

(20) Sánchez-Sánchez, M. C.; Navarro, R. M.; Fierro, J. L. G. Ethanol Steam Reforming Over Ni/M$_x$ O$_y$-Al$_2$O$_3$ (M=Ce, La, Zr And Mg) Catalysts: Influence Of Support On The Hydrogen Production. *Int. J. Hydrogen Energy* **2007**, *32*, 1462−1471.

(21) Bouarab, R.; Akdim, O.; Auroux, A.; Cherifi, O.; Mirodatos, C. Effect Of Mgo Additive On Catalytic Properties Of Co/SiO$_2$ In The Dry Reforming Of Methane. *Appl. Catal., A* **2004**, *264*, 161−168.

(22) Wei, J.; Iglesia, E. Isotopic And Kinetic Assessment Of The Mechanism Of Reactions Of CH$_4$ With CO$_2$ Or H$_2$O To Form Synthesis Gas And Carbon On Nickel Catalysts. *J. Catal.* **2004**, *224*, 370−383.

(23) Ligthart, D. A. J. M.; van Santen, R. A.; Hensen, E. J. M. Influence Of Particle Size On The Activity And Stability In Steam Methane Reforming Of Supported Rh Nanoparticles. *J. Catal.* **2011**, *280*, 206−220.

(24) Theofanidis, S. A.; Galvita, V. V.; Poelman, H.; Marin, G. B. Enhanced Carbon-Resistant Dry Reforming Fe-Ni Catalyst: Role Of Fe. *ACS Catal.* **2015**, *5*, 3028−3039.

(25) You, X.; Wang, X.; Ma, Y.; Liu, J.; Liu, W.; Xu, X.; Peng, H.; Li, C.; Zhou, W.; Yuan, P.; Chen, X. Ni-Co/Al$_2$O$_3$ bimetallic Catalysts For CH$_4$ steam Reforming: Elucidating The Role Of Co For Improving Coke Resistance. *ChemCatChem* **2014**, *6*, 3377−3386.

(26) Gao, X.; Tan, Z.; Hidajat, K.; Kawi, S. Highly Reactive Ni-Co/SiO$_2$ Bimetallic Catalyst Via Complexation With Oleylamine/Oleic Acid Organic Pair For Dry Reforming Of Methane. *Catal. Today* **2017**, *281*, 250−258.

(27) Bian, Z.; Kawi, S. Highly Carbon-Resistant Ni−Co/Sio$_2$ Catalysts Derived From Phyllosilicates For Dry Reforming Of Methane. *J. CO2 Util.* **2017**, *18*, 345−352.

(28) Li, Z.; Mo, L.; Kathiraser, Y.; Kawi, S. Yolk−Satellite−Shell Structured Ni−Yolk@Ni@SiO$_2$ Nanocomposite: Superb Catalyst toward Methane CO$_2$ Reforming Reaction. *ACS Catal.* **2014**, *4*, 1526−1536.

(29) Li, Z.; Kathiraser, Y.; Ashok, J.; Oemar, U.; Kawi, S. Simultaneous Tuning Porosity and Basicity of Nickel@Nickel−Magnesium Phyllosilicate Core−Shell Catalysts for CO$_2$ Reforming of CH$_4$. *Langmuir* **2014**, *30*, 14694−14705.

(30) Price, C. A. H.; Earles, E.; Pastor-Pérez, L.; Liu, J.; Reina, T. R. Advantages Of Yolk Shell Catalysts For The DRM: A Comparison Of Ni/ZnO@SiO$_2$ Vs. Ni/CeO$_2$ And Ni/Al$_2$O$_3$. *Chemistry* **2019**, *1*, 3−16.

(31) Mohamedali, M.; Henni, A.; Ibrahim, H. Recent Advances In Supported Metal Catalysts For Syngas Production From Methane. *Chem. Eng.* **2018**, *2*, 9.

(32) Bian, Z.; Das, S.; Wai, M. H.; Hongmanorom, P.; Kawi, S. A Review on Bimetallic Nickel-Based Catalysts for CO$_2$ Reforming of Methane. *ChemPhysChem* **2017**, *18*, 3117−3134.

(33) Zhang, J.; Wang, H.; Dalai, A. K. Effects Of Metal Content On Activity And Stability Of Ni-Co Bimetallic Catalysts For CO$_2$ Reforming Of CH$_4$. *Appl. Catal., A* **2008**, *339*, 121−129.

(34) AlSabban, B.; Falivene, L.; Kozlov, S. M.; Aguilar-Tapia, A.; Ould-Chikh, S.; Hazemann, J.-L.; Cavallo, L.; Basset, J.-M.; Takanabe, K. In-Operando Elucidation Of Bimetallic CoNi Nanoparticles During High-Temperature CH$_4$/CO$_2$ Reaction. *Appl. Catal., B* **2017**, *213*, 177−189.

(35) Bonifacio, C. S.; Carenco, S.; Wu, C. H.; House, S. D.; Bluhm, H.; Yang, J. C. Thermal Stability Of Core−Shell Nanoparticles: A Combined In Situ Study By XPS And TEM. *Chem. Mater.* **2015**, *27*, 6960−6968.

(36) Carenco, S.; Wu, C.-H.; Shavorskiy, A.; Alayoglu, S.; Somorjai, G. A.; Bluhm, H.; Salmeron, M. Synthesis And Structural Evolution Of Nickel-Cobalt Nanoparticles Under H$_2$ and CO$_2$. *Small* **2015**, *11*, 3045−3053.

(37) Wu, Z.; Yang, B.; Miao, S.; Liu, W.; Xie, J.; Lee, S.; Pellin, M. J.; Xiao, D.; Su, D.; Ma, D. Lattice Strained Ni-Co Alloy As a High-Performance Catalyst For Catalytic Dry Reforming Of Methane. *ACS Catal.* **2019**, *9*, 2693−2700.

(38) De, S.; Zhang, J.; Luque, R.; Yan, N. Ni-Based Bimetallic Heterogeneous Catalysts For Energy And Environmental Applications. *Energy Environ. Sci.* **2016**, *9*, 3314−3347.

(39) Wang, L.; Li, D.; Koike, M.; Watanabe, H.; Xu, Y.; Nakagawa, Y.; Tomishige, K. Catalytic Performance And Characterization Of Ni−Co Catalysts For The Steam Reforming Of Biomass Tar To Synthesis Gas. *Fuel* **2013**, *112*, 654−661.

(40) Takanabe, K.; Nagaoka, K.; Nariai, K.; Aika, K.-i. Titania-Supported Cobalt And Nickel Bimetallic Catalysts For Carbon Dioxide Reforming Of Methane. *J. Catal.* **2005**, *232*, 268−275.

(41) Creemer, J. F.; Santagata, F.; Morana, B.; Mele, L.; Alan, T.; Iervolino, E.; Pandraud, G.; Sarro, P. M. An All-In-One Nanoreactor For High-Resolution Microscopy On Nanomaterials At High

Pressures. In *2011 IEEE 24th International Conference on Micro Electro Mechanical Systems*; IEEE: 2011.

(42) Vendelbo, S. B.; Elkjær, C. F.; Falsig, H.; Puspitasari, I.; Dona, P.; Mele, L.; Morana, B.; Nelissen, B. J.; van Rijn, R.; Creemer, J. F.; Kooyman, P. J.; Helveg, S. Visualization Of Oscillatory Behaviour Of Pt Nanoparticles Catalysing CO Oxidation. *Nat. Mater.* **2014**, *13*, 884−890.

(43) Bremmer, G. M.; Zacharaki, E.; Sjåstad, A. O.; Navarro, V.; Frenken, J. W. M.; Kooyman, P. J. In Situ TEM Observation Of The Boudouard Reaction: Multi-Layered Graphene Formation From CO On Cobalt Nanoparticles At Atmospheric Pressure. *Faraday Discuss.* **2017**, *197*, 337−351.

(44) van Ravenhorst, I. K.; Vogt, C.; Oosterbeek, H.; Bossers, K. W.; Moya-Cancino, J. G.; van Bavel, A. P.; van der Eerden, A. M. J.; Vine, D.; de Groot, F. M. F.; Meirer, F.; Weckhuysen, B. M. Capturing The Genesis Of An Active Fischer-Tropsch Synthesis Catalyst With Operando X-Ray Nanospectroscopy. *Angew. Chem., Int. Ed.* **2018**, *57*, 11957−11962.

(45) de Smit, E.; Swart, I.; Creemer, J. F.; Hoveling, G. H.; Gilles, M. K.; Tyliszczak, T.; Kooyman, P. J.; Zandbergen, H. W.; Morin, C.; Weckhuysen, B. M.; de Groot, F. M. F. Nanoscale Chemical Imaging Of A Working Catalyst By Scanning Transmission X-Ray Microscopy. *Nature* **2008**, *456*, 222−225.

(46) Menezes, P. W.; Indra, A.; Levy, O.; Kailasam, K.; Gutkin, V.; Pfrommer, J.; Driess, M. Using Nickel Manganese Oxide Catalysts For Efficient Water Oxidation. *Chem. Commun.* **2015**, *51*, 5005−5008.

(47) Al Samarai, M.; Hahn, A. W.; Beheshti Askari, A. B.; Cui, Y.-T.; Yamazoe, K.; Miyawaki, J.; Harada, Y.; Rüdiger, O.; DeBeer, S. Elucidation Of Structure−Activity Correlations In A Nickel Manganese Oxide Oxygen Evolution Reaction Catalyst By Operando Ni L-Edge X-Ray Absorption Spectroscopy And 2P3d Resonant Inelastic X-Ray Scattering. *ACS Appl. Mater. Interfaces* **2019**, *11*, 38595−38605.

(48) Raberg, L. B.; Jensen, M. B.; Olsbye, U.; Daniel, C.; Haag, S.; Mirodatos, C.; Sjastad, A. O. Propane Dry Reforming To Synthesis Gas Over Ni-Based Catalysts: Influence Of Support And Operating Parameters On Catalyst Activity And Stability. *J. Catal.* **2007**, *249*, 250−260.

(49) Chen, D.; Christensen, K.; Ochoafernandez, E.; Yu, Z.; Totdal, B.; Latorre, N.; Monzon, A.; Holmen, A. Synthesis Of Carbon Nanofibers: Effects Of Ni Crystal Size During Methane Decomposition. *J. Catal.* **2005**, *229*, 82−96.

(50) Kim, J.-H.; Suh, D. J.; Park, T.-J.; Kim, K.-L. Effect Of Metal Particle Size On Coking During CO_2 Reforming Of CH_4 Over Ni−Alumina Aerogel Catalysts. *Appl. Catal., A* **2000**, *197*, 191−200.

(51) Al-Fatesh, A. S. A.; Fakeeha, A. H. Effects Of Calcination And Activation Temperature On Dry Reforming Catalysts. *Journal of Saudi Chemical Society* **2012**, *16*, 55−61.

(52) Tillmann, L.; Schulwitz, J.; van Veen, A.; Muhler, M. Dry Reforming Of Methane At High Pressure In A Fixed-Bed Reactor With Axial Temperature Profile Determination. *Catal. Lett.* **2018**, *148*, 2256−2262.

(53) Raabe, J.; Tzvetkov, G.; Flechsig, U.; Böge, M.; Jaggi, A.; Sarafimov, B.; Vernooij, M. G. C.; Huthwelker, T.; Ade, H.; Kilcoyne, D.; Tyliszczak, T.; Fink, R. H.; Quitmann, C. Pollux: A New Facility For Soft X-Ray Spectromicroscopy At The Swiss Light Source. *Rev. Sci. Instrum.* **2008**, *79*, 113704.

(54) Flechsig, U.; Quitmann, C.; Raabe, J.; Böge, M.; Fink, R.; Ade, H. The Pollux Microspectroscopy Beam Line At The Swiss Light Source. In *AIP Conference Proceedings*; American Institute of Physics: 2007.

(55) Cesário, M. R., Gennequin, C.; Abi-Aad, E.; de Macedo, D. *Catalytic Materials For Hydrogen Production And Electro-Oxidation Reactions. Frontiers In Ceramic Science*; Bentham Science Publishers: 2018, Volume 2, p140.

(56) Moongraksathum, B.; Shang, J.-Y.; Chen, Y.-W. Photocatalytic Antibacterial Effectiveness Of Cu-Doped TiO_2 Thin Film Prepared Via The Peroxo Sol-Gel Method. *Catalysts* **2018**, *8*, 352.

(57) Zhang, X.; Liu, J.; Jing, Y.; Xie, Y. Support Effects On The Catalytic Behavior Of NiO/Al_2O_3 For Oxidative Dehydrogenation Of Ethane To Ethylene. *Appl. Catal., A* **2003**, *240*, 143−150.

(58) Nyathi, T. M.; Fischer, N.; York, A. P. E.; Claeys, M. Effect of crystallite size on the performance and phase transformation of Co_3O_4/Al_2O_3 catalysts during CO-PrOx − an *in situ* study. *Faraday Discuss.* **2017**, *197*, 269−285.

(59) Wang, H.-Y.; Hung, S.-F.; Chen, H.-Y.; Chan, T.-S.; Chen, H. M.; Liu, B. In Operando Identification Of Geometrical-Site-Dependent Water Oxidation Activity Of Spinel Co_3O_4. *J. Am. Chem. Soc.* **2016**, *138*, 36−39.

(60) Cesário, M. R.; Gennequin, C.; Abi-Aad, E.; de Macedo, D. A. *Catalytic Materials For Hydrogen Production And Electro-Oxidation Reactions*; Bentham Science Publishers: Sharjah, 2018, *1*.

(61) Wang, D.; Li, S.; Du, Y.; Wu, X.; Chen, Y. Self-Templating Synthesis Of 3D Hierarchical $NiCo_2O_4@NiO$ Nanocage From Hydrotalcites For Toluene Oxidation. *Catalysts* **2019**, *9*, 352.

(62) Jeangros, Q.; Hansen, T. W.; Wagner, J. B.; Damsgaard, C. D.; Dunin-Borkowski, R. E.; Hébert, C.; Van herle, J.; Hessler-Wyser, A. Reduction Of Nickel Oxide Particles By Hydrogen Studied In An Environmental TEM. *J. Mater. Sci.* **2013**, *48*, 2893−2907.

(63) Faes, A.; Nakajo, A.; Hessler-Wyser, A.; Dubois, D.; Brisse, A.; Modena, S.; Van herle, J. Redox Study Of Anode-Supported Solid Oxide Fuel Cell. *J. Power Sources* **2009**, *193*, 55−64.

(64) Zhang, J.; Wang, H.; Dalai, A. K. Development Of Stable Bimetallic Catalysts For Carbon Dioxide Reforming Of Methane. *J. Catal.* **2007**, *249*, 300−310.

(65) Fan, X.; Liu, Z.; Zhu, Y.-A.; Tong, G.; Zhang, J.; Engelbrekt, C.; Ulstrup, J.; Zhu, K.; Zhou, X. Tuning the composition of metastable $Co_x Ni_y Mg_{100−x−y}(OH)(OCH_3)$ nanoplates for optimizing robust methane dry reforming catalyst. *J. Catal.* **2015**, *330*, 106−119.

(66) Wolfbeisser, A.; Sophiphun, O.; Bernardi, J.; Wittayakun, J.; Föttinger, K.; Rupprechter, G. Methane Dry Reforming Over Ceria-Zirconia Supported Ni Catalysts. *Catal. Today* **2016**, *277*, 234−245.

(67) Bang, S.; Hong, E.; Baek, S. W.; Shin, C.-H. Effect of acidity on Ni catalysts supported on P-modified Al_2O_3 for dry reforming of methane. *Catal. Today* **2018**, *303*, 100−105.

(68) Nagaoka, K.; Takanabe, K.; Aika, K.-i. Modification Of Co/TiO_2 For Dry Reforming Of Methane At 2Mpa By Pt, Ru Or Ni. *Appl. Catal., A* **2004**, *268*, 151−158.